Journal of Alloys and Compounds 507 (2010) 386–390

Contents lists available at ScienceDirect

Journal of Alloys and Compounds

journal homepage: www.elsevier.com/locate/jallcom

Raman scattering from ZnO incorporating Fe nanoparticles: Vibrational modes and low-frequency acoustic modes

N. Romčević[a,*], R. Kostić[a], B. Hadžić[a], M. Romčević[a], I. Kuryliszyn-Kudelska[b], W.D. Dobrowolski[b], U. Narkiewicz[c], D. Sibera[c]

[a] Institute of Physics, University of Belgrade, Pregrevica 118, 11080 Belgrade, Serbia
[b] Institute of Physics PAS, Al. Lotnikow 32/46, 02/668 Warsaw, Poland
[c] Szczecin University of Tehnology, Institute of Chemical and Environmental Engineering, Puleskiego 10, 70-322 Szczecin, Warsaw, Poland

ARTICLE INFO

Article history:
Received 31 May 2010
Received in revised form 30 July 2010
Accepted 4 August 2010
Available online 11 August 2010

Keywords:
Nanostructured materials
Optical properties
Light absorption and reflection

ABSTRACT

Nanocrystaline samples of ZnO(Fe) were synthesized by wet chemical method. Samples were characterized by X-ray diffraction to determine composition of the samples (ZnO, Fe_2O_3, $ZnFe_2O_4$) and the mean crystalline size (8–52 nm). In this paper we report the experimental spectra of Raman scattering. Main characteristics of experimental Raman spectrum in 200–1600 cm^{-1} spectral region are: sharp peak at 436 cm^{-1} and broad two-phonon structure at ~1150 cm^{-1}, typical for ZnO; broad structure below 700 cm^{-1} that has different position and shape in case of $ZnFe_2O_4$ or Fe_2O_3 nanoparticles. Low-frequency Raman modes were measured and assigned according to confined acoustic vibrations of spherical nanoparticles. Frequencies of these vibrational modes were analyzed in elastic continuum approximation, which considers nanoparticle as homogeneous elastic sphere.

1. Introduction

Recently, a continued interest in the synthesis and properties of nanoscale inorganic materials has been observed. Semiconductor nanocrystals have been of much interest over two decades because of their unique physical properties resulting from modification of the electronic states due to the confinement effect. Currently, nanostructures made of ZnO have attracted significant attention owing to their proposed applications in low-voltage and short-wavelength electro-optical devices, transparent ultraviolet protection films, and spintronic devices [1,2].

A considerable attention has recently been devoted to high temperature ferromagnetism observed in transition metal doped oxides. Particularly ZnO has been identified as a promising host semiconductor material, exhibiting ferromagnetism when doped with most of the transition metals – V, Cr, Fe, Co, Ni [3]. However, the origin of ferromagnetic behavior is not very well known in these compounds. Recently, it was shown that the ferromagnetism in these materials can be induced by inclusions of nanoscale oxides of transition metals [4] and/or nanoparticles containing a large concentration of magnetic ions [5]. Novel methods enabling a control of nanoassembling of magnetic nanocrystals in nonconducting matrices as well as functionalities specific to such systems were described [5].

2. Samples and characterization

The nanocrystalline samples of ZnO doped Fe_2O_3 were synthesized by co-precipitation method [6]. First, the mixture of iron hydroxides and zinc hydroxides from an aqueous solution of nitrites were obtained. Next, the obtained hydroxides were filtered, dried at the temperature of 70 °C and calcined at 300 °C during 1 h. The series of samples containing from 5 to 95 wt.% of Fe_2O_3 was obtained. In the present paper we present the results of micro-Raman studies and low-frequency Raman modes measurements for two selected samples with low (5 wt.%) and high (90 wt.%) content of magnetic dopant.

The structural properties of the samples were studied by means X-ray diffraction technique ($Co_{K\alpha}$ radiation, X'Pert Philips). The performed XRD measurements allowed for the phase composition determination and to determine a mean crystallite size d in prepared samples by use of Scherrer's formula [7]. The detailed studies of structural properties by means of XRD technique were presented in Ref. [6]. The crystalline phases of hexagonal ZnO, rhombohedric Fe_2O_3 and cubic $ZnFe_2O_4$ were identified as presented in [6]. The mean crystalline size of these phases is given in Table 1 in Ref. [6]. For sample with 5 wt.% of Fe_2O_3, assigned as $(ZnO)_{0.95}(Fe_2O_3)_{0.05}$, crystalline phase of $ZnFe_2O_4$ is identified. Mean crystallite size is

* Corresponding author. Tel.: +381 11 3713 026; fax: +381 11 7313 052.
E-mail address: romcevi@ipb.ac.rs (N. Romčević).

0925-8388/$ – see front matter © 2010 Elsevier B.V. All rights reserved.
doi:10.1016/j.jallcom.2010.08.013

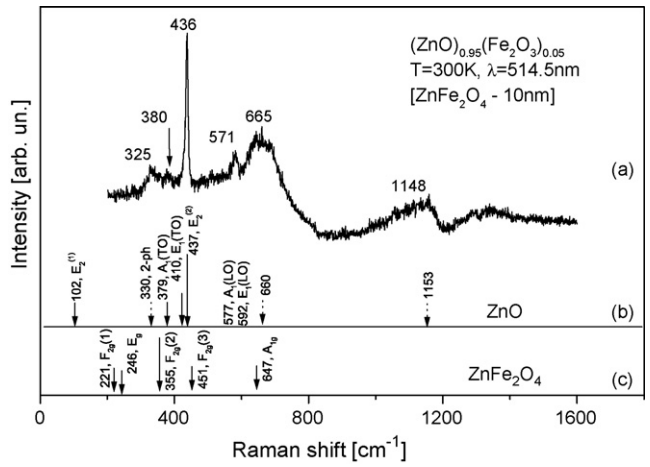

Fig. 1. Raman spectra of nanocrystaline ZnO doped with 5 wt.% of Fe_2O_3 assigned as $(ZnO)_{0.95}(Fe_2O_3)_{0.05}$.

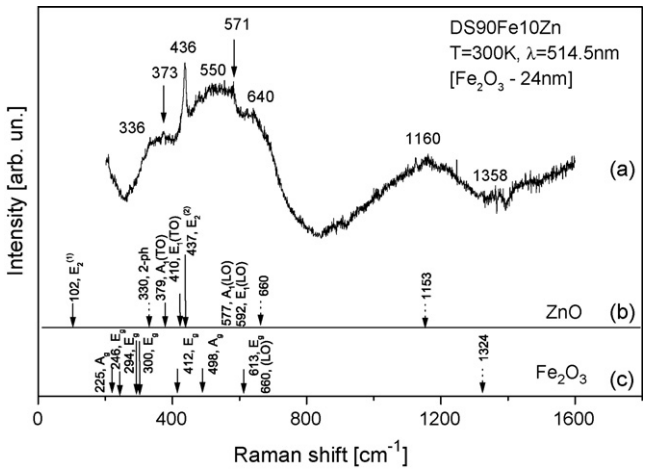

Fig. 2. Raman spectra of nanocrystaline ZnO doped with 90 wt.% of Fe_2O_3 assigned as DS90Fe10Zn.

$a = 10$ nm. The second sample with 90 wt.% of Fe_2O_3 is assigned as DS90Fe10Zn, crystallite of Fe_2O_3 is identified with mean crystallite size $a = 24$ nm. No other crystal phases are observed in these samples.

XRD measurements did not reveal presence of ZnO phase in these samples. It is interesting that for the samples with lower concentration of Fe_2O_3 (up to 20 wt.% of Fe_2O_3) exitonic lines from ZnO are observed. In some samples, for instance sample containing 40 wt.% of Fe_2O_3, crystallites of ZnO and $ZnFe_2O_4$ are identified [6].

3. Results and discussion

3.1. Raman spectroscopy

The micro-Raman spectra were taken in the backscattering configuration and analyzed using Jobin Yvon T64000 spectrometer, equipped with nitrogen cooled charge-coupled-device detector. As excitation source we used the 514.5 nm line of an Ar–iron laser. The measurements were performed at different laser power. Fig. 1(a) Raman spectra of nanocrystaline ZnO doped with 5 wt.% of Fe_2O_3 assigned as $(ZnO)_{0.95}(Fe_2O_3)_{0.05}$ is presented.

We will start analysis of spectrum in Fig. 1 with brief report about structure and vibrational properties of potentially present materials in sample. Vibrational properties of bulk material are crucial for understanding vibrational properties of small particles. As consequence of miniaturization, we expect bulk modes to be shifted and broadened.

Basic material in this research is ZnO. ZnO is a semiconductor with a wurtzite crystal structure. This hexagonal structure belongs to the space group $C_{6v}{}^4$, with two formula units per primitive cell, where all atoms occupy C_{3v} sites. The optical phonons at the center of the Brillouin zone belong to the following irreducible representations: $\Gamma_{opt} = A_1 + 2B_1 + E_1 + 2E_2$. Modes of symmetry A_1, E_1 and E_2 are Raman active, and A_1 and E_1 are infrared active. B_1 are inactive (silent) modes. Both A_1 and E_1 are polar modes and split into transverse (TO) and longitudinal (LO) phonons with different frequencies due to macroscopic electric fields associated with the LO phonons. The short-range interatomic forces cause anisotropy. That is why A_1 and E_1 modes have different frequencies. As the electrostatic forces dominate the anisotropy in the short-range forces, the TO–LO splitting is larger than the A_1–E_1 splitting. For the lattice vibration A_1 atoms move parallel to the c-axis and for E_1 perpendicular to c-axis. Two nonpolar Raman active modes, are often assigned as $E_2{}^{(1)}$(low) and $E_2{}^{(2)}$(high). All these modes have been reported in the Raman scattering spectra of bulk ZnO many times [8,9]. Frequencies and assignation of Raman active modes in ZnO are presented on the bottom of Fig. 1(b). Solid lines indicate A_1, E_1 and E_2 phonon modes in ZnO. Dashed lines mark multi-phonon scattering at ~330 cm^{-1}, ~655 cm^{-1} and ~1153 cm^{-1} (2LO).

$ZnFe_2O_4$ spinel has a cubic structure that belongs to the space group $O_h{}^7$. Full unit cell contains eight formula units, and primitive cell contains two formula units. The optical phonons at Γ-point of the Brilluene zone belong to the following irreducible representations: $\Gamma_{opt} = A_{1g} + E_g + F_{1g} + 3F_{2g} + 2A_u + 2E_u + 4F_{1u} + 2F_{2u}$. There are five first order active Raman modes: A_{1g}, E_g and $3F_{2g}$. Modes F_{1u} are infrared-active. In the cubic spinels, including ferrites, the modes above 600 cm^{-1} mostly correspond to the motion of oxygen atoms in tetrahedral AO_4 group. The other lower frequency modes represent the characteristic of the octahedral BO_6 sites. Frequencies [10] and assignations of Raman–active modes in $ZnFe_2O_4$ are presented on the bottom of Fig. 1(c).

Dispute the fact that XRD does not evident ZnO, sharp peak in our spectrum at 436 cm^{-1} is clearly $E_2{}^{(2)}$ mode of ZnO. Position is practically the same as in bulk material. Phonon dispersion relation, that corresponds to the $E_2{}^{(2)}$ mode in ZnO at the Γ point, does not show considerable dispersion. So, even in ZnO nanoparticle spectra position of this mode is practically unchanged. Peak at ~571 cm^{-1}, is identified as LO ZnO mode. Also structure at ~1150 cm^{-1} can be prescribed to multiphonon 2LO mode in ZnO. Wide and dominant structure centered at 665 cm^{-1} corresponds to vibrations in the tetrahedral AO_4 group. Materials like: Mn_3O_4, Fe_3O_4, Co_3O_4 have Raman active mode in interval 600–700 cm^{-1}. Even in bulk $ZnFe_2O_4$ three the most intensive Raman modes at 355 cm^{-1}, 451 cm^{-1} and 647 cm^{-1} exhibit broad characteristics. If there is any disorder of the Zn and Fe cations in the tetrahedral and octahedral sites, the vibrations related to the two types of cations at the same site may result in two separated first order Raman modes. If they are very close in frequency an overlapped broad peak should be observed.

Raman spectrum in region below 400 cm^{-1} is superposition of characteristic frequencies of ZnO phase and spectrum of $ZnFe_2O_4$ nanoparticles. In bulk $ZnFe_2O_4$ mode at 355 cm^{-1} is strong and wide, and modes at 221 cm^{-1} and 246 cm^{-1} are week. In $ZnFe_2O_4$ nanoparticles these modes are wider and contribute to high level of spectral curve.

Raman spectra of nanocrystaline ZnO doped with 90 wt.% of Fe_2O_3 assigned as DS90Fe10Zn is presented in Fig. 2. Only nanoparticles of Fe_2O_3 are registered by XRD.

We will give brief report about structure and vibrational properties of Fe_2O_3. Fe_2O_3 crystallize in the rhombohedric (trigonal) system with space group $D_{3d}{}^6$. Primitive unit cell contains two

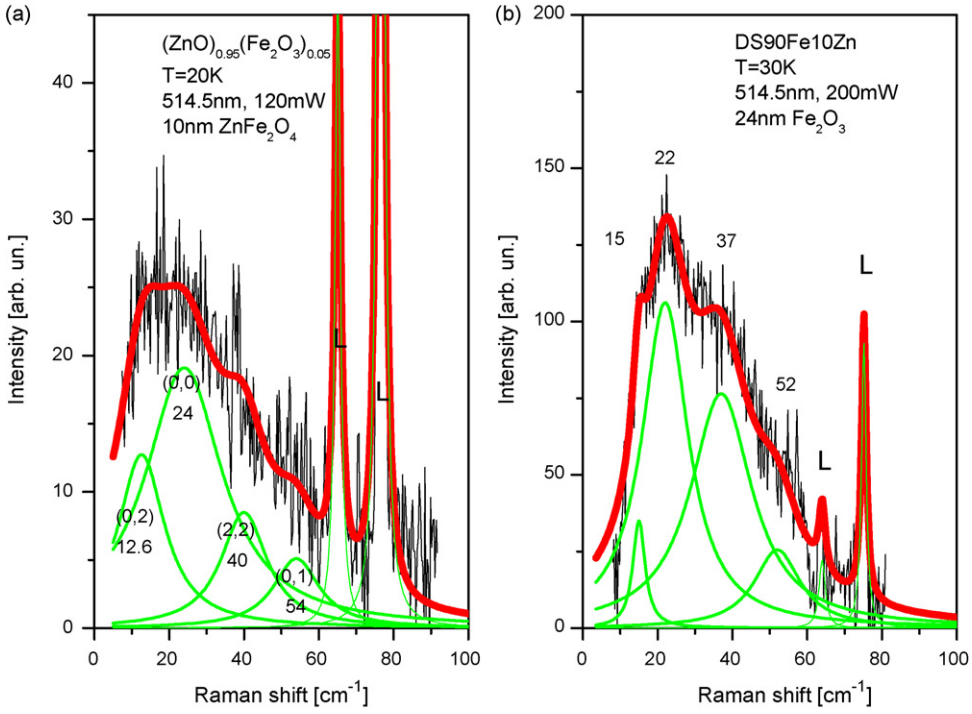

Fig. 3. Low-frequency Raman spectra of sample: (a) $(ZnO)_{0.95}(Fe_2O_3)_{0.05}$ where $ZnFe_2O_4$ crystallites of $a = 10$ nm size are identified, (b) DS90Fe10Zn where Fe_2O_3 crystalites of $a = 24$ nm size are identified.

formula units. The optical phonons at the Γ-point of the Brilluene zone belong to the following irreducible representations: $\Gamma = 2A_{1g} + 2A_{1u} + 3A_{2g} + 2A_{2u} + 5E_g + 4E_u$. $2A_{1g}$ and $5E_g$ are Raman active modes. $2A_{2u}$ and $4E_u$ modes are infrared active. Information about Fe_2O_3 Raman spectra are presented at the bottom of Fig. 2(c) [11–13]. In edition to these first order Raman spectra there is a very prominent peak at ∼1320 cm^{-1}. LO phonon situated at ∼660 cm^{-1} is Raman forbidden. It can be activated, and become visible, if symmetry rules are broken. The 2LO mode which is Raman allowed is seen in all the spectra. Strength of this mode is remarkable in case of resonance.

ZnO mode at 436 cm^{-1}, LO ZnO mode at ∼571 cm^{-1} and ZnO multiphonon mode at ∼1160 cm^{-1} can easily be identified. In spectral region below 400 cm^{-1} there is superposition of ZnO phase and Fe_2O_3 nanoparticles spectrum. Difference of spectra in Figs. 1 and 2, in region below 400 cm^{-1}, is consequence of presence of $ZnFe_2O_4$ (Fig. 1) or Fe_2O_3 (Fig. 2) nanoparticles.

3.2. Low-frequency Raman spectroscopy

The Raman spectra were excited by the 514.5 nm line of an Ar laser (the average power was about 120 mW) in the backscattering geometry. We used Jobin Yvon model U-1000 monochromator, with a conventional photocounting system. In order to make low-frequency Raman modes visible we subtracted the intensity of the elastic scattering background by A/ω^n approximation. Resulted Raman spectra are presented in Fig. 3. The observed modes are deconvoluted using the Lorentzian line profile.

Low-frequency modes are analyzed as confined acoustic vibrations of nanoparticles. The frequencies of acoustic vibrational modes can be calculated in the elastic continuum approximation. Parameters of the model are stiffnes constants and mass density of the particle material. In doped samples $ZnFe_2O_4$ and Fe_2O_3 structures are identified. As the dimension of the particles is already determined and having in mind specific frequency to diameter dependence, we established material parameters and analyzed behavior of nanoparticles.

Transverse (v_T) and longitudinal (v_L) sound velocity are parameters of equation of motion of the three-dimensional elastic body. Transverse and longitudinal sound velocity are directly connected to stiffness constants and the mass density. If we assume that nanoparticles are small spheres, equation of motion must be solved in spherical coordinate. It is useful to introduce dimensionless variables $\eta = \omega R/v_T = \omega d/2v_T$ and $\xi = \omega R/v_L = \omega d/2v_L$ where R is radius of the particle (d is diameter). Boundary conditions definitely determine the solutions [14–18].

If one assumes that there is no displacement at the particle surface, it is so-called rigid boundary conditions. If one assumes that there is no force on the surface, i.e. radial components of the stress tensor at the surface are zero, it is so-called free-surface boundary conditions. We assumed the stress-free boundary conditions [17]. We believe that this model is adequate to describe behavior of nanoparticles in our samples, as there is no compact matrix surrounding them.

In spherical case, each value of angular momentum quantum number l($l = 0,1,2,..$) gives a series of solutions. We numerate these solutions n($n = 0,1,2,..$). So, eigen solutions are labeled as η^{nl} (ξ^{nl}), and eigen states are labeled as (n,l). Two types of vibrational modes are obtained: spheroidal and torsional modes. As $\omega^{nl} = 2\eta^{nl}v_T/d$ i.e. $\omega^{nl} = 2\xi^{nl}v_L/d$, each solution gives one linear dependence $\omega^{nl} = f(1/d)$.

Dimensionless solutions of equation for spheroidal modes strongly depend on the material through ratio v_L/v_T. Solutions for torsional modes, do not depend on material. According to the group theory analysis the spheroidal $l = 0$ and $l = 2$ modes are Raman active [19]. Theory implies [20] that the spheroidal mode (0,0) is the most intensive in the $l = 0$ series, and the most intensive of all Raman active modes. In a lot of experimental spectra only this mode was detected. The first quadropolar mode is the most intensive in $l = 2$ series. The frequency of (0,2) mode is almost always lower than the (0,0) mode frequency.

Structure of $ZnFe_2O_4$ is similar to Fe_3O_4. In analysis of $ZnFe_2O_4$ we started from Fe_3O_4 acoustic properties. For Fe_3O_4 of spinel (cubic) structure we used following parameters: mass

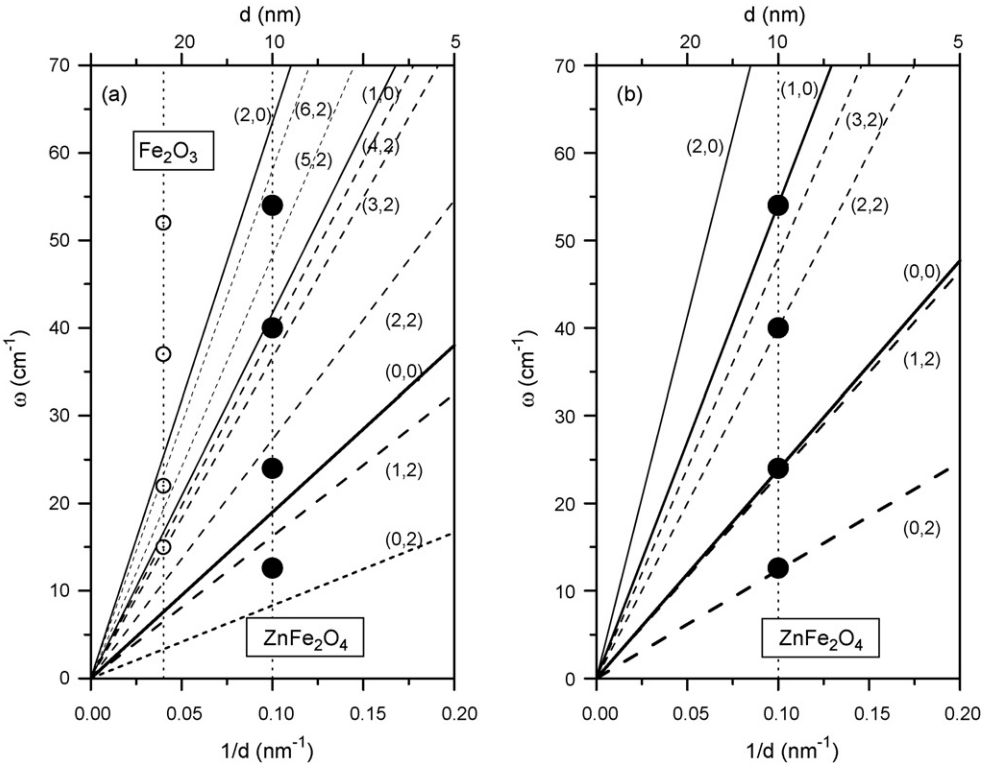

Fig. 4. (a) Dependence of eigen solutions, for spheroidal modes in the surface stress-free approximation, on Fe_3O_4 nanoparticles inverse diameter: $v_L = 6400$ m/s and $v_T = 2960$ m/s. Plotted lines represent eigen solutions. Solid and opened cycles are experimental results of $ZnFe_2O_4$ and Fe_2O_3 respectively. (b) Dependence of eigen solutions on nanoparticles inverse diameter: $v_L = 8355$ m/s and $v_T = 4397$ m/s. Solid cycles are experimental results of $ZnFe_2O_4$.

density 5240 kg/m^3 and stiffness constants $C_{11} = 2.17 \times 10^{11}$ N/m^2, $C_{12} = 1.21 \times 10^{11}$ N/m^2, $C_{44} = 0.46 \times 10^{11}$ N/m^2 [21]. Longitudinal and transverse sound velocities in a case of cubic crystal are: $v_L = (C_{11}/\rho)^{1/2} = 6400$ m/s and $v_T = (C_{44}/\rho)^{1/2} = 2960$ m/s. Solutions for Fe_3O_4, in case of stress-free boundary conditions, for the $l = 0$, $n = 0,1,2$ and $l = 2$, $n = 0,1,2,3,4$ are presented in Fig. 4(a)). We marked (solid cycles) positions of frequencies that are result of deconvolution of $ZnFe_2O_4$ particles experimental spectra. First two frequencies, 12.6 cm^{-1} and 24 cm^{-1}, that are the best defined structures in spectra, are located very close to Fe_3O_4 (0,0) and (0,2) solutions, i.e. lines in Fig. 4(a). Also mode at ≈24 cm^{-1} is more intensive than mode at ≈12.6 cm^{-1}, Fig. 3(a).

We tentatively attributed mode at 24 cm^{-1}, Fig. 3(a), to be ω^{00} (0,0) and mode at 12.6 cm^{-1}, Fig. 3(a), to be ω^{02} (0,2). As $\omega^{00} = 2\xi^{00} v_L/d$ and $\omega^{02} = 2\eta^{02} v_T/d = 2\xi^{02} v_L/d$ follows that $\omega^{00}/\omega^{02} = \xi^{00}/\xi^{02} = 1.9$. From curves ξ^{00} (v_L/v_T) and ξ^{02} (v_L/v_T) function $g(v_L/v_T) = \xi^{00}$ $(v_L/v_T)/\xi^{02}$ (v_L/v_T) can be established. As $\omega^{00}/\omega^{02} = 1.9$, from $g(v_L/v_T)$ follows that $v_L/v_T = 1.9$ and $\xi^{00}(1.9) = 2.68$. From $\omega^{00} = 24$ cm^{-1} $d = 10$ nm follows: $v_L = 8355$ m/s and $v_T = v_L/1.9 = 4397$ m/s. These are new parameters that can be prescribed to $ZnFe_2O_4$. We solved complete problem with these new parameters. New solutions are as lines presented in Fig. 4(b).

Basic assumption was that $\omega^{00} = 24$ cm^{-1} and $\omega^{02} = 12.6$ cm^{-1}. As we see $\omega^{12} \approx \omega^{00}$, Fig. 4(b) and cannot be separated and detected in experimental spectra. Band at ≈40 cm^{-1} is identified as (2,2) and band at ≈54 cm^{-1} as (1,0) mode. Very good agreement between experimental and calculated results, Fig. 4(b), imply that our assumptions were correct.

In Fig. 4(a) we marked (open cycles) frequency positions that are result of experimental Fe_2O_3 particles spectra deconvolution ($d = 24$ nm) Fig. 3(b). As expected experimental frequencies are far away from calculated Fe_3O_4 values, Fig. 4(a). For cubic system it is reasonable to use effective i.e. averaged parameters, as we did for Fe_3O_4 and $ZnFe_2O_4$. α-Fe_2O_3 crystallize in rhombohedric (trigonal) system, conventionally viewed as hexagonal. Stiffness constants, and consequently sound velocities, differ very much for different crystallographic axes in α-Fe_2O_3 and from Fe_3O_4 values. It was not reasonable to follow the procedure with averaged parameters as in $ZnFe_2O_4$. To established parameter of material that determined low-frequency Raman spectra of Fe_2O_3 more detailed analysis is needed.

4. Conclusion

Small amount (5 wt.%) of Fe_2O_3 at the beginning of the synthesis results in forming of $ZnFe_2O_4$ nanoparticles. Large amount (90 wt.%) of Fe_2O_3 at the beginning of the synthesis results in forming Fe_2O_3 nanoparticles. Both samples contain ZnO phase which is not registered by XRD, but is clearly seen in the Raman spectra. In low-frequency Raman spectra of $ZnFe_2O_4$ nanoparticles registered peaks agree well with the calculated frequencies of acoustic phonons. As a result we identified (0,2), (0,0), (2,2) and (1,0) modes

Acknowledgements

This work was supported under the Agreement of Scientific Collaboration between Polish Academy of Science and Serbian Academy of Sciences and Arts. The work in Serbia was supported by Serbian Ministry of Science (Projects No. 141028) and supported by Research Network WITNANO and Polish Ministry for Higher Education and Science.

References

[1] Y. Chen, D.M. Bagnall, H. Koh, K. Park, K. Higara, Z. Zhu, T. Yao, J. Appl. Phys. 84 (1988) 3912.
[2] J. Nemeth, G. Rodriguez-Gattorno, A. Diaz, I. Dekany, Langmuir 20 (2004) 2855.
[3] J.M.D. Coey, M. Venkatesan, C.B. Fitzgerald, Nat. Mater. 4 (2005) 173.

[4] C. Sudakar, J.S. Thakur, G. Lawes, R. Naik, V.M. Naik, Phys. Rev. B 75 (2007) 054423.
[5] T. Dietl, Acta Phys. Pol. A 111 (2007) 27.
[6] U. Narkiewicz, D. Sibera, I. Kuryliszyn-Kudelska, L. Kilanski, W.N. Dobrowolski, Romcevic Acta Phys. Pol. A 113 (2008) 1695.
[7] A.L. Patterson, Phys. Rev. 56 (1993) 978.
[8] N. Ashkenov, B.N. Mbenkum, C. Bundesmann, V. Riede, M. Lorenz, D. Spemann, E.M. Kaidashev, A. Kasic, M. Shubert, M. Grundmann, J. Appl. Phys. 93 (2003) 126.
[9] E.F. Venger, A.V. Melnichuk, L. Lu Melnichuk, Yu A. Pasechuk, Phys. Status Solidi B 188 (1995) 823.
[10] Z. Wang, D. Schiferl, Y. Zhao, H.St.C. O'Neill, J. Phys. Chem. Solids 64 (2003) 2517.
[11] F Bauciuman, F. Patcas, R. Craciun, D.R.T. Zahn, Phys. Chem. Chem. Phys. 1 (1999) 185.
[12] O.N. Shebanova, P. Lazar, J. Solid State Chem. 174 (2003) 424.
[13] V.G. Hajdiev, M.N. Iliev, I.V. Vergilov, J. Phys. C: Solid State Phys. 21 (1988) 1199.
[14] A. Tanaka, S. Onari, T. Arai, Phys. Rev. B 47 (1993) 1237.
[15] L. Saviot, B. Champagnon, E. Duval, A.I. Ekimov, Phys. Rev. B 57 (1998) 341.
[16] L. Saviot, D.B. Murray, M. del, C. Marco de Lucas, Phys. Rev. B 69 (2004) 113402.
[17] L. Saviot, B. Champagnon, E. Duval, I.A. Kudriavtsev, I.E. Akimov, J. Non-Cryst. Solids 197 (1996) 238.
[18] E. Roca, C. Trallero-Giner, M. Cardona, Phys. Rev. B 49 (1994) 13704.
[19] E. Duval, Phys. Rev. B 46 (1992) 5795.
[20] N. Combe, J.R. Huntzinger, A. Mlayah, Phys. Rev. B 76 (2007) 205425.
[21] P. Nordlander, M. Ronay, Phys. Rev. B 36 (1987) 4982.